ATTITUDE PROPAGATION FROM DIGITAL IMAGES

Roberto V. F. Lopes, Adenilson R. Silva and Hélio K. Kuga

INPE, C.P. 515, 12201-970 São José dos Campos, SP, Brazil, e-mail: roberto.lopes@dss.inpe.br

ABSTRACT

In this paper one introduces an innovative attitude propagation system for remote sensing satellites based on a series of overlapped images taken from a digital camera on the satellite. The system aims to relief the ground control software from the need of identifying landmarks in every payload image and is not based on the expensive and sensitive gyro technology. The attitude propagation procedure starts by fitting a space correlation model to the first image of the series. Then the "kriging" technique is used to predict the next image of the series, as a function of its position and attitude small shifts. The attitude shift is such that the predicted image matches the next taken image. The accuracy of the procedure is evaluated by digital simulation with realistic Earth's surface patterns. Numerical results are presented as a function of the image resolution. They give a preliminary idea about the system feasibility envisaging its experimental implementation in space.

1. INTRODUCTION

In this paper one analyses the feasibility of an innovative attitude propagation system for Earth oriented satellites based on the Active Pixel Sensor (APS/CMOS) technology. The system relies on the fact that the satellite three-axis attitude can be propagated from a sequence of overlapped images of the Earth surface taken from a digital camera. The system aims to relief the ground control software of remote sensing missions from the need of identifying landmarks in every payload image. Nonetheless, it can as well be applied to any Earth oriented mission where an attitude propagation system not based on the expensive and sensitive gyro technology could be considered advantageous. This includes a range of scientific micro satellites with stringent funding budgets.

The compactness level achieved by the APS/CMOS technology combined with the increasing capacity of digital processors and an observed global trend to get more science from less money has already encouraged similar developments and studies in this field ([1], [2], and [3]). This paper introduces the use of a deterministic-stochastic hybrid model to the image sequence in order to estimate the satellite three-axis rotation. This model consists of two distinct components: one deterministic and one stochastic. The deterministic component is a linear combination of an orthogonal function basis in the two-dimensional focal plane coordinates system. It represents the overall trend of the image. The stochastic component captures the image details that are space correlated in some extent. The coefficients of the deterministic component and the space covariance kernel of the stochastic component are both estimated from the observed image frames by least squares. Once the model is fitted, the "kriging" technique (see Dubrule, for instance) of Geostatistics is used to predict the next image of the sequence, as a linear function of its position and attitude small shifts. In principle both attitude and position shifts could be jointly estimated, but the satellite position is supposed to be known within a negligible error level. This assumption is compatible with the accuracy of currently available GPS receivers. Then, the attitude shift is estimated by matching the predicted image with the next taken image. The accuracy of the procedure is evaluated by digital simulation based on real satellite images with different resolutions and surface patterns. A trade off between the camera characteristics and the system performance gives a preliminary idea about the system feasibility envisaging its experimental implementation in future space missions.

2. NOMENCLATURE

t_k	k-th sample time
$r_{\circ,k}$	Satellite position vector at t_k in the Earth reference system WGS84
v_k	Satellite velocity vector at t_k in the Earth reference system WGS84
A_k	Satellite attitude matrix at t_k
w_k	Satellite angular velocity with respect to the WGS84 at t_k in the body frame
dq_k	Rotation vector corresponding to the satellite rotation from t_k to t_{k+1}
w_E	Earth angular rate
$P_{i,j}$	The (i,j) active pixel
$S_{i,j,k}$	Earth surface area corresponding to the pixel $P_{i,j}$ at t_k
$Ds_{i,j,k}$	Size of $S_{i,j,k}$
$r_{i,j,k}$	Position vector of $S_{i,j,k}$, in the Earth reference system WGS84
$r_{i,j,k}$	Distance from $S_{i,j,k}$ to the satellite at t_k
$n_{i,j,k}$	Unit vector normal to $S_{i,j,k}$
$a_{i,j,k}$	Coelevation of the satellite as seen from $S_{i,j,k}$ at t_k
$y_{i,j,k}$	Diffuse radiation from $S_{i,j,k}$ at t_k in the

	camera spectral band
$f_\circ$	Maximum diffuse radiation flux from $S_{i,j,k}$ at t_k in the camera spectral band
$f_{i,j,k}$	Diffuse radiation flux from $S_{i,j,k}$ to the satellite, in the camera spectral band at t_k
$p_{i,j}$	Two dimensional coordinates of $P_{i,j}$ in the focal plane frame: $p_{i,j} \equiv \{x_j \quad y_i\}'$
e	Unit vector normal to the focal plane in the body frame
U	Base of the focal plane frame written in the body frame
N	Number of active pixels
L	Size of the set of active pixels
$\Delta\ell$	Size of each active pixel
f	Focal length
D	Diameter of the optical system aperture
$u_{i,j}$	Line of sight unit vector of $P_{i,j}$ in the body frame
$t_{i,j}$	Tilt of $u_{i,j}$ with respect to e
$d_{i,j}$	Distance from $P_{i,j}$ to the optical center
$\Delta s_{i,j}$	Solid angle of $S_{i,j,k}$ as seen from the satellite at t_k
$\Delta a_{i,j,k}$	Solid angle of the optical system lens as seen from $S_{i,j,k}$ at t_k
$I_{i,j,k}$	Radiation incident to $P_{i,j}$ at t_k in the camera spectral band.

3. MAPPING THE EARTH SURFACE

The digital camera is composed of an optical system, a matrix of active pixels and the associated electronics. The optical system maps the Earth's surface in its field of view to the matrix of active pixels on the focal plane. It may include a set of lenses and optical filters. The active pixels convert the incident energy in their sensitive spectral band into electrical signals. The electronics amplifies, samples, digitalizes and stores the intensity of those signals. Figure 1 illustrates the mapping geometry for a digital camera with a single lens, where $t_{i,j} = s_{i,j}$.

The radiation incident to an active pixel $P_{i,j}$ at sample time t_k in the camera spectral band is given by:

$$I_{i,j,k} = f_{i,j,k}\, \Delta a_{i,j,k}\, \Delta s_{i,j,k} \tag{1}$$

Where $f_{i,j,k}$, $\Delta a_{i,j,k}$ and $\Delta s_{i,j,k}$ are given by:

$$f_{i,j,k} = f_\circ \cos a_{i,j,k} \tag{2}$$

$$\Delta a_{i,j,k} = \frac{p}{2} D^2\, r_{i,j,k}^{-2} \cos s_{i,j} \tag{3}$$

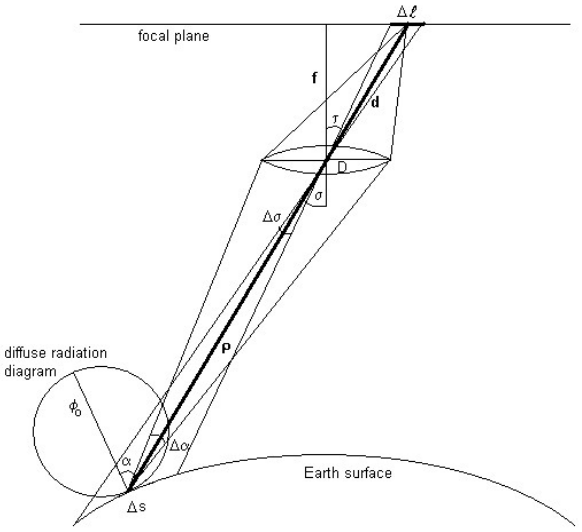

Figure 1 – Geometry of the Earth surface mapping by a digital camera.

$$\Delta s_{i,j,k} = \frac{r_{i,j,k}^2}{\cos a_{i,j,k}}\, d_{i,j}^{-2}\, \Delta\ell\, \cos t_{i,j} \tag{4}$$

and the distance $d_{i,j}$ is:

$$d_{i,j} = \frac{f}{\cos t_{i,j}} \tag{5}$$

The diffuse radiation is the space integration of the diffuse radiation flux over the hemisphere:

$$y_{i,j,k} = \int_0^{\frac{1}{2}p} \int_0^{2p} f(a) \sin a \; dj \; da = 2p f_\circ \int_0^{\frac{1}{2}p} \cos a \sin a \; da = p \; f_\circ \tag{6}$$

Therefore, the output of the active pixel $P_{i,j}$ at sample time t_k can be written as:

$$g_{i,j,k} = h_{i,j}\, y_{i,j,k}\, \frac{L D^2}{2N f^2} \cos^3 t_{i,j} \cos s_{i,j} \tag{7}$$

Where $h_{i,j}$ represents the linear transfer function of the active pixel $P_{i,j}$.

Ideally, $h_{i,j}$ should be the same for every pixel. However, real digital cameras present non-uniformities. Also, pixels close to the edge of the field of view may experiment the signal attenuation expressed by the cosine terms in Equation 7. Furthermore, the optical system may present optical aberrations and non-linear distortions, besides the unavoidable diffraction. These practical aspects must be taken into account in a real application. Nevertheless, for the sake of the paper focus, one considers here that they are as much as possible compensated in a pre-processing phase by means of a calibration effort.

So, one define the calibrated output as:

$$\tilde{g}_{i,j,k} \equiv \frac{2N f^2}{LD^2} \frac{g_{i,j,k}}{h_{i,j,k}} \cos^{-3} t_{i,j} \cos^{-1} s_{i,j} = y_{i,j,k} + e_{i,j,k} \tag{8}$$

where $e_{i,j,k}$ is a random noise that represents the combined effect of thermal noises, residuals of the calibration process, diffraction and presence of non diffuse radiation.

4. THE IMAGE SPACE MODEL

In order to interpolate the image at any position p, one defines a space function g_k such that:

$$g_k(p_{i,j}) = \tilde{g}_{i,j,k} . \tag{9}$$

Following the kriging approach, natural phenomena characterized by space density functions can be described as a combination of deterministic and stochastic components:

$$g_k(p) \equiv \bar{g}_k(p) + dg_k(p) . \tag{10}$$

The deterministic component gives a smooth, overall description of the phenomenon large-scale characteristics. Fine details are given by the stochastic component. Both model components are described below.

4.1. Large-Scale Image Model

The deterministic function selected to describe the large-scale image characteristics is a modified series of Fourier:

$$\bar{g}_k(p) = C_{0,0} + \sum_b C_{0,b} \cos bp\tilde{x} + \sum_a C_{a,0} \cos ap\tilde{y} + \\ + \sum_a \sum_b C_{a,b} \cos bp\tilde{x} \cos ap\tilde{y},$$
$$\forall \tilde{x} \in [0,1], \quad \forall \tilde{y} \in [0,1], \tag{11}$$

where

$$C_{0,0} = \frac{1}{4XY} \int_{-Y}^{Y} \int_{-X}^{X} g(x,y)\, dx\, dy \cong \frac{1}{N} \sum_i \sum_j \tilde{g}_{i,j,k} , \tag{12a}$$

$$C_{0,b} = 2\int_0^1 \int_0^1 g(\tilde{x},\tilde{y}) \cos bp\tilde{x}\, d\tilde{x}\, d\tilde{y} \\ \cong \frac{2}{N} \sum_i \sum_j \tilde{g}_{i,j,k} \cos bp\tilde{x}_j , \tag{12b}$$

$$C_{a,0} = 2\int_0^1 \int_0^1 g(\tilde{x},\tilde{y}) \cos ap\tilde{y}\, d\tilde{x}\, d\tilde{y} \\ \cong \frac{2}{N} \sum_i \sum_j \tilde{g}_{i,j,k} \cos ap\tilde{y}_i , \tag{12c}$$

$$C_{a,b} = 4\int_0^1 \int_0^1 g(\tilde{x},\tilde{y}) \cos bp\tilde{x} \cos ap\tilde{y}\, d\tilde{x}\, d\tilde{y} \\ \cong \frac{4}{N} \sum_i \sum_j \tilde{g}_{i,j,k} \cos bp\tilde{x}_j \cos ap\tilde{y}_i , \tag{12d}$$

and $\tilde{x} \equiv \frac{1}{2}(x+X)\, X^{-1}$, $\tilde{y} \equiv \frac{1}{2}(y+Y)\, Y^{-1}$.

The order of the series depends on the number of pixels and the image pattern. Undersized orders yield poor interpolations with smooth biases. Oversized orders penalize the computational effort without a correspondent gain in the interpolation quality and may even add a false roughness pattern to the image. The final choice is taken empirically.

4.2. Short Scale Image Model

The stochastic component of the image model is characterized by an unbiased noise with space correlation function R_k:

$$E\{dg_k(p)\} = 0 , \tag{13}$$

$$E\{dg_k(p)\, dg_k(p+dp)\} = R_k(|dp|) , \tag{14}$$

where $E\{\cdot\}$ is the expectance operator.

The correlation function is expanded in Taylor's series:

$$R_k(h) = X_\circ + \sum_{m>0} X_m \frac{h^m}{m!} . \tag{15}$$

The order of the series is chosen empirically and the coefficients X_m are fitted by least squares from the real image data. Usually, if the deterministic model component has a suitable order the correlation decays with the distance. Furthermore, the stochastic model is supposed to represent the short-scale image characteristics only. Therefore, one defines a correlation domain $\Re_{i,j}$ around each image pixel such that only the pixels inside this domain need to be taken into account in the sampling correlation evaluations described in this section.

4.3. Image Interpolation

Once the parameters of both large-scale and short-scale image models are determined, the image can be interpolated as follows. From Equation 11 one can directly interpolate the deterministic image component. The interpolation of the stochastic image component can only be estimated as a linear combination of the observed image in the correlation domain $\Re_{i,j}$ of the closest image pixel to the desired position p:

$$d\hat{g}_k(p) = \sum_{\forall\{i',j'\} | P_{i',j'} \in \Re_{i,j}} c_{i',j'} \left[\tilde{g}_{i',j',k} - \bar{g}_k(p_{i',j'})\right] ,$$

$$\{i,j\}:\left|p_{i,j}-p\right|=\min_{i',j'}\left\{\left|p_{i',j'}-p\right|\right\}, \tag{16}$$

where the coefficients $c_{i',j'}$ have to minimize the variance of the interpolation residual:

$$\min_{c_{i',j'}} E\left\{\left[dg_k(p)-d\hat{g}_k(p)\right]^2\right\}. \tag{17}$$

Let $Q_{i,j}$ be a matrix where each column is the position vector $p_{i',j'}$ of a pixel $P_{i',j'}\in\Re_{i,j}$, in a given order; $l_{i,j}$ a vector where each row is given by the correspondent value of $\tilde{g}_{i',j',k}-\bar{g}_k(p_{i',j'})$; $m_{i,j}$ a vector where each row is given by the correspondent value of $c_{i',j'}$; $z_{i,j}$ a vector where each row is given by the correspondent value of the correlation $R_k\left(\left|p-p_{i,j}\right|\right)$; and L a matrix with elements (a,b) given by the correlation between the elements a and b of matrix $Q_{i,j}$:

$$\left(\mathrm{L}_{i,j}\right)_{a,b}=R_k\left(h_{a,b}\right),\quad h_{a,b}^2=\mathrm{Q}_{a,a}-2\,\mathrm{Q}_{a,b}+\mathrm{Q}_{b,b},$$
$$\mathrm{Q}\equiv Q'_{i,j}\,Q_{i,j}. \tag{18}$$

Then, the interpolation function $d\hat{g}_k$ may be written as:

$$d\hat{g}_k(p)=l'_{i,j}m_{i,j}, \tag{19}$$

where $m_{i,j}$ is the solution of $\min_{m_{i,j}}\left\{\mathrm{X}_\circ-2\,z'_{i,j}m_{i,j}+\mathrm{L}\right\}$:

$$m_{i,j}=\mathrm{L}^{-1}\,z_{i,j}. \tag{20}$$

Therefore, the image interpolation function is finally given by:

$$\hat{g}_k(p)=\bar{g}_k(p)+l'_{i,j}\,\mathrm{L}^{-1}\,z_{i,j}(p) \tag{21}$$

It may be verified that $\hat{g}_k(p_{i,j})=\tilde{g}_{i,j,k}$, $\forall i,j$. Also, $\hat{g}_k$ is a nonlinear function of p. A linearized expression for $\hat{g}_k$ is given by:

$$\hat{g}_k(p)\cong\tilde{g}_{i,j,k}+\nabla\hat{g}_k(p_{i,j})\left(p-p_{i,j}\right), \tag{22}$$

where

$$\nabla\hat{g}_k=\nabla\bar{g}_k+l'_{i,j}\,\mathrm{L}^{-1}\,\nabla z_{i,j} \tag{23}$$

and the gradients of $\bar{g}_k$ and $z_{i,j}$ are given below:

$$\frac{\partial\bar{g}_k}{\partial x}=-\sum_b\frac{\mathrm{b}p}{2\mathrm{X}}\sin bp\tilde{\mathrm{x}}\left\{C_{0,b}+\sum_a C_{a,b}\cos ap\tilde{y}\right\},$$

$$\frac{\partial\bar{g}_k}{\partial y}=-\sum_a\frac{\mathrm{a}p}{2\mathrm{Y}}\sin ap\tilde{\mathrm{y}}\left\{C_{a,0}+\sum_b C_{a,b}\cos bp\tilde{x}\right\},$$

$$\left(\nabla z_{i,j}\right)_\ell=\left\{\sum_{m>0}\mathrm{X}_m\frac{h_a^{m-2}}{(m-1)!}\right\}\left\{p-\left(Q_{i,j}\right)_\ell\right\}',\quad h_\ell=\left|p-\left(Q_{i,j}\right)_\ell\right| \tag{24}$$

5. IMAGE DYNAMIC MODEL

As the satellite moves from one sample time to the next one, the image changes slightly. More specifically, a surface element $S_{i,j,k}$ is mapped into the image pixel $P_{i,j}$ at sample time t_k. At the next sample time, that same surface element would be mapped into a pseudo pixel slightly shifted with respect to $P_{i,j}$. The amount of this shift as a function of the satellite attitude and orbit displacements is derived below.

The line of sight unit vector of $S_{i,j,k}$ at t_k in the body frame is a function of $u_{i,j}$ and e that depends of the design of the optical system. In the case illustrated in Figure 1, it is given by:

$$u_{i,j}=A_k\,\frac{r_{i,j,k}-r_{\circ,k}}{r_{i,j,k}}, \tag{25}$$

where

$$r_{i,j,k}=\left|r_{i,j,k}-r_{\circ,k}\right|. \tag{26}$$

At t_{k+1} the satellite attitude matrix and its position change to:

$$A_{k+1}=\exp\left\{-\mathrm{W}(dq_k)\right\}A_k\cong A_k-\mathrm{W}(dq_k)A_k \tag{27}$$

$$r_{\circ,k+1}=r_{\circ,k}+dr_k, \tag{28}$$

where $\mathrm{W}(\cdot)$ is the vector product operator, and

$$dr_k=v_k\left(t_{k+1}-t_k\right)-\mathrm{W}(w_E)\,r_{\circ,k}. \tag{29}$$

Consequently, the distance from $S_{i,j,k}$ to the satellite and the satellite line of sight unit vector change respectively by:

$$dr_{i,j,k}=-\frac{\left(r_{i,j,k}-r_{\circ,k}\right)'}{r_{i,j,k}}dr_k, \tag{30}$$

$$du_{i,j,k}=\mathrm{W}\left(u_{i,j}\right)dq_k-\left[I-u_{i,j}\,u'_{i,j}\right]A_k\,\frac{dr_k}{r_{i,j,k}}. \tag{31}$$

The relation between the position vector $p_{i,j}$ of a given pixel in the focal plane and the correspondent unit vector $u_{i,j}$ is given by:

$$u_{i,j} = \left(f^2 + p'_{i,j}\ p_{i,j}\right)^{-\frac{1}{2}} \begin{Bmatrix} p_{i,j} \\ f \end{Bmatrix}, \tag{32}$$

$$p_{i,j} = \frac{U' u_{i,j}}{e' u_{i,j}}\ f\ . \tag{33}$$

Therefore, a displacement $du_{i,j,k}$ in the line of sight corresponds to a displacement $dp_{i,j,k}$ in the focal plane:

$$dp_{i,j,k} = \left(\frac{f\ U - e\ p'_{i,j}}{e' u_{i,j}} \right)' du_{i,j,k} \tag{34}$$

Let $F_{i,j,k}$ and $H_{i,j}$ be the matrices defined by:

$$F_{i,j,k} \equiv \left(\frac{f\ U - e\ p'_{i,j}}{e' u_{i,j}} \right)' \frac{A_k}{r_{i,j,k}} \tag{35}$$

$$H_{i,j} \equiv \left(\frac{f\ U - e\ p'_{i,j}}{e' u_{i,j}} \right)' \mathrm{W}\left(u_{i,j}\right) \tag{36}$$

It follows that:

$$dp_{i,j,k} = F_{i,j,k}\ dr_k + H_{i,j}\ dq_k \tag{37}$$

Now, the image at t_{k+1} obeys:

$$g_{k+1}\left(p_{i,j} + dp_{i,j,k}\right) = \tilde{g}_{i,j,k}\,, \tag{38}$$

Thus, in view of equations 22 and 37, equation 38 yields:

$$\tilde{g}_{i,j,k} \cong \tilde{g}_{i,j,k+1} + \left\{\nabla \hat{g}_{k+1}(p_{i,j})\right\}\left(F_{i,j,k}\ dr_k + H_{i,j}\ dq_k\right) \tag{39}$$

6. ATTITUDE PROPAGATION

Equation 39 can be rewritten as a rotation vector observation equation:

$$d\tilde{g}_{i,j,k} = \mathrm{G}_{i,j,k}\ dq_k + n_{i,j,k} \tag{40}$$

where $n_{i,j,k}$ represents the observation noise, and:

$$d\tilde{g}_{i,j,k} \equiv \tilde{g}_{i,j,k} - \tilde{g}_{i,j,k+1} - \left\{\nabla \hat{g}_{k+1}(p_{i,j})\right\} F_{i,j,k}\ dr_k \tag{41}$$

$$\mathrm{G}_{i,j,k} \equiv \left\{\nabla \hat{g}_{k+1}(p_{i,j})\right\} H_{i,j} \tag{42}$$

The rotation vector dq_k is then estimated by least squares from the set of observations $d\tilde{g}_{i,j,k}$:

$$\begin{aligned} \min_{dq_k} J &\equiv \sum_{\forall i,j} \left(d\tilde{g}_{i,j,k} - \mathrm{G}_{i,j,k}\ dq_k\right)^2 \\ &= dq'_k\ B_k\ dq_k - 2\ b'_k\ dq_k + K \end{aligned}, \tag{43}$$

where:

$$K \equiv \mathrm{tr}\left(dG_k\ dG'_k\right), \tag{44}$$

$$b_k \equiv \begin{Bmatrix} \mathrm{tr}\left(dG_k\ \mathrm{G}'_{x,k}\right) \\ \mathrm{tr}\left(dG_k\ \mathrm{G}'_{y,k}\right) \\ \mathrm{tr}\left(dG_k\ \mathrm{G}'_{z,k}\right) \end{Bmatrix}, \tag{45}$$

$$\mathrm{B_k} \equiv \begin{pmatrix} \mathrm{tr}\left(\mathrm{G}_{x,k}\ \mathrm{G}'_{x,k}\right) & \mathrm{tr}\left(\mathrm{G}_{x,k}\ \mathrm{G}'_{y,k}\right) & \mathrm{tr}\left(\mathrm{G}_{x,k}\ \mathrm{G}'_{z,k}\right) \\ \mathrm{tr}\left(\mathrm{G}_{y,k}\ \mathrm{G}'_{x,k}\right) & \mathrm{tr}\left(\mathrm{G}_{y,k}\ \mathrm{G}'_{y,k}\right) & \mathrm{tr}\left(\mathrm{G}_{y,k}\ \mathrm{G}'_{z,k}\right) \\ \mathrm{tr}\left(\mathrm{G}_{z,k}\ \mathrm{G}'_{x,k}\right) & \mathrm{tr}\left(\mathrm{G}_{z,k}\ \mathrm{G}'_{y,k}\right) & \mathrm{tr}\left(\mathrm{G}_{z,k}\ \mathrm{G}'_{z,k}\right) \end{pmatrix} \tag{46}$$

and dG_k, $\mathrm{G}_{x,k}$, $\mathrm{G}_{y,k}$ and $\mathrm{G}_{z,k}$ are the matrices with components i, j given respectively by $d\tilde{g}_{i,j,k}$, the first, second and third elements of $\mathrm{G}_{i,j,k}$.

The estimate of dq_k is:

$$\hat{dq}_k = B_k^{-1}\ b_k\ . \tag{47}$$

7. NUMERICAL RESULTS

In order to have a preliminary evaluation of the predicted performance of the attitude propagation from the proposed algorithm, 24 images taken by different remote sensing satellites and from places with six different surface patterns were processed. Because images taken by remote sensing satellites have a far better resolution than the expected with digital cameras, their resolution was intentionally degraded in the simulations. Furthermore, the simulations considered only attitude motions, since the orbit motion is considered perfectly known.

The simulations were carried out trough the steps described below:

i. The high-resolution digital image was converted to a real matrix of size $\mathrm{N_x} \times \mathrm{N_y}$;
ii. A low-resolution image was then simulated at sample time t_1 by sample averaging subsets of the original image, each with size 15×15;
iii. Similarly, a low-resolution image was simulated at sample time t_2, by sample averaging the subsets of the original image shifted by a $dp_{i,j}$ correspondent to the given rotation dq (since the resolution of the original image is much better than the simulated one, the quantization error on $dp_{i,j}$ has little effect here);
iv. The coefficients of the Fourier series fitting the simulated images were evaluated;
v. The coefficients of the correlation function were evaluated from the residuals of the deterministic

model considering a square correlation domain 15×15;

vi. The coefficients of the image prediction model are then evaluated;

vii. The attitude prediction error is evaluated.

Some typical results are shown in Figures 2 and 3, while Figure 4 summarizes the results of the whole images set. In most cases the attitude propagation error was in the range from 1'' to 30''. The larger the number of pixels, the smaller is the dispersion of the results. The surface patterns did not seem to have any meaningful rule in the results.

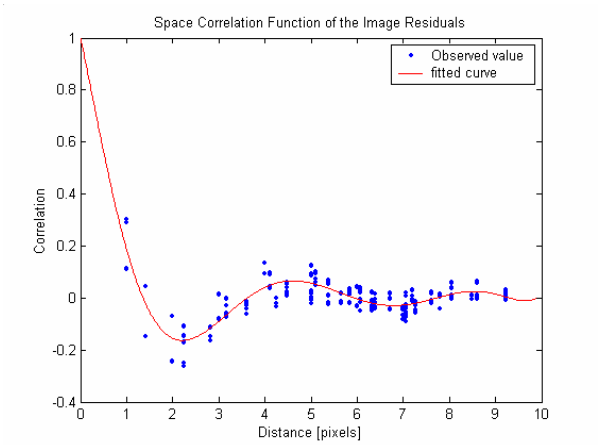

Figure 2 – The space correlation function

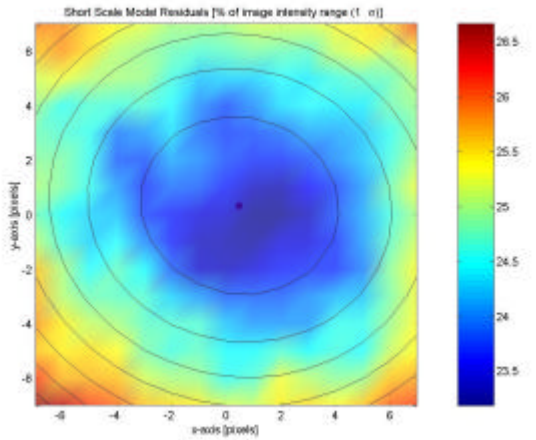

Figure 3 – The rms of image prediction residual.

8. FINAL COMMENTS AND CONCLUSIONS

An algorithm for attitude propagation was presented based on digital images. The algorithm was tested using real images taken from different remote sensing satellites and with different image patterns. As well known, cumulative attitude propagation errors cause an attitude drift that asks for calibration using absolute attitude sensors. As a consequence, the final attitude accuracy is better than the accuracy of the absolute sensor alone, the degree of the improvement being determined by the magnitude of the attitude drift. The accuracy of the attitude propagation depends on the image resolution but not to the image pattern.

The algorithm has some control parameters that need to be set empirically based on extensive tests. There are several other aspects to be investigated envisaging a future implementation of the algorithm, like the effects of darkness during the night, cloudy images, sampling frequency, etc. The amount of tests carried out up to now did not intend to be conclusive, but only to give an indication about the concept feasibility.

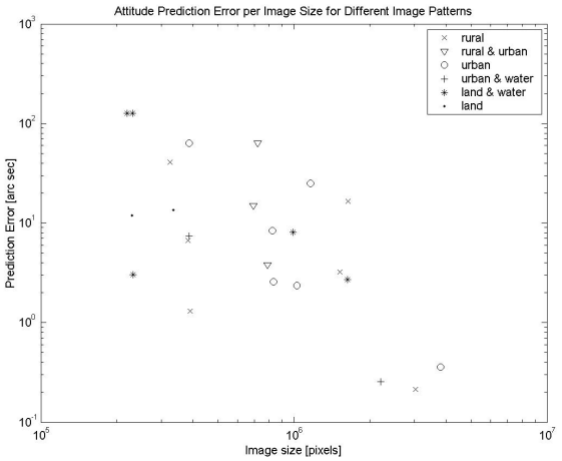

Figure 4 – Attitude prediction errors for representative image patterns as a function of the image size.

REFERENCES

1. Barraza, J. F. and Grzywacz, N. M. "Local Computation of Angular Velocity in Rotational Visual Motion." *J. Opt. Soc. Am. A*, Vol. 20, No. 7, July 2003, pp.1382-1390.

2. Janschek, K. and Dyblenko, S. "Satellite Autonomous Navigation Based on Image Motion Analysis". *Space Technology*, Vol. 21, No. 4, pp. 157-162, 2001.

3. Meller, D.; Sripruetkiat, P and Makove, K. "Digital CMOS Cameras for Attitude Determination." (paper SSC00-VII-1) *Proc. of 14th Annual AIAA/USU Conf. on Small Satellites*, North Logan, UT, USA, Aug. 2000.

4. Dubrule, O. "Two Methods with Different Objectives: Splines and Kriging." *Jour. Math. Geol.*, Vol. 15, pp. 245-257.